Yin *et al. Int J Concr Struct Mater (2018) 12:50*
https://doi.org/10.1186/s40069-018-0282-3

International Journal of Concrete Structures and Materials

ORIGINAL ARTICLE

Open Access

Analysis of Active Ion-Leaching Behavior and the Reaction Mechanism During Alkali Activation of Low-Calcium Fly Ash

Bo Yin[1,2], Tianhe Kang[1*], Jianting Kang[1] and Yuejuan Chen[1,2]

Abstract

The dissolution and release of active ions, such as Si^{4+}, Al^{3+} and Ca^{2+}, from fly ash directly affect the rate and extent of reaction product formation, which in turn affect the physical and mechanical properties of fly ash filling materials. In this study, low-calcium fly ash was soaked and activated in NaOH solutions with different concentrations (approximating the optimum dose range) for different lengths of time. The amounts of active ions leached and the changes in the mineral composition, chemical functional groups and surface morphology were tested and analyzed via ICP-OES, XRD, FTIR and SEM/EDS techniques. Based on these analyses, the reaction mechanism of alkali activation of low-calcium fly ash was further investigated. The results showed that the NaOH activation effect can significantly increase the amount of active ions leached from low-calcium fly ash. Notably, the amount of Si^{4+} and Al^{3+} leached clearly increased with increases in both NaOH concentration and soaking time. The plausible reaction mechanism is discussed in detail, which is that the alkali activator principally affected the surface of the vitreous particles of low-calcium fly ash and induced differing surface modifications in the dissolution stage, depolymerization stage, polycondensation and polymer gel stage and diffusion stage. It was observed that the progress of the reaction is controlled by dissolution in the early stages, whereas activation is governed by diffusion when the surfaces of the fly ash particles are covered by precipitates.

Keywords: low-calcium fly ash, alkali activation, leaching behavior, reaction mechanism

1 Introduction

Fly ash has been widely used as a building material and as a component in products such as cement, concrete products, construction products, bridge engineering products and geopolymers (Blissett and Rowson 2012; Çiçek and Cincin 2015; Kotwal et al. 2015; Kim et al. 2016; Roychand et al. 2016). In recent decades, fly ash has generally been used as a raw material in mine paste backfilling (MPB) in China. The addition of fly ash can enhance the performance of filling material, decrease engineering costs, improve filling material workability, and reduce pumping power requirements. This MPB technology provides a green solution for utilizing fly ash and avoids the negative impact of this material on the environment and ecosystems (Qian et al. 2007). However, when fly ash filling materials were introduced, the replacement of Portland cement with fly ash, especially in high volumes, was found to result in serious defects, such as low early strength and large deformations. These defects directly affect the ability of the material to control ground subsidence. Previous research has showed that this low early strength is due to the slow pozzolanic reaction activity of fly ash (Shi 1996). Therefore, increasing the pozzolanic activity of fly ash is helpful for improving the early physical and mechanical properties of fly ash filling material.

A number of approaches for accelerating the pozzolanic activity of fly ash have been investigated (Shi 2001; Guo et al. 2014; Nikolić et al. 2014). Many authors have found that the addition of chemical activators can effectively accelerate the pozzolanic reactivity of fly ash and increase the convenience of chemical activation, and such

*Correspondence: kangtianhe18@163.com
[1] Institute of Mining Technology, Taiyuan University of Technology, Taiyuan 030024, China
Full list of author information is available at the end of the article
Journal information: ISSN 1976-0485 / eISSN 2234-1315

methods are also cost effective. These chemical activators include acid activators, alkaline activators, sulfate activators, and chloride activators (Shi and Day 1993; Palomo et al. 1999; Guerrero et al. 2000; Fernández-Jiménez and Palomo 2005; Fernandez-Jimenez et al. 2007; Rashad 2014; Zhang et al. 2016). The clear consensus is that fly ash is an acidic material containing acidic oxides, and because of its pozzolanic reactivity in alkaline medium, it most likely requires activation (Xie and Xi 2001). Therefore, alkaline activators have a more noticeable effect than other types of activators. Moreover, reports have indicated that among such alkaline activators, NaOH treatment has the best activation effect on fly ash (Bijen and Waltje 1989; Shi et al. 2005). At the same time, some authors noted that the dose of the alkali activator has a considerable influence on the material strength. No clear activation effect occurs when the dose is small, whereas the strength of the material is reduced when the dose is too large, because the material strength decreases as the amount of the alkali activator in the mixture increases; thus, an optimum dose exists (Purdon 1940; Tango 1992; Shi et al. 2005; Luan et al. 2010).

Alkali-activated fly ash promotes the release of active Si^{4+} and Al^{3+} ions via decomposition of the dense silicon–aluminum network structure (Ma et al. 2012; Khalifeh et al. 2015; Zhuang et al. 2016). The behavior of leached active ions in the pozzolanic reaction process and the formation of reaction products have important impacts. The leaching behavior of low-calcium fly ash in the presence of optimal doses of alkali activators in filling material has not yet been studied in detail. In addition, the leaching of ions and the subsequent formation of reaction products during this period of the development process is not well understood. The exploration of these problems is considered to be valuable in reducing the dose and cost of alkali activators and for promoting the widespread field application of alkali activators in MPB technology.

Thus, the present study evaluated the amount of active ions, such as Si^{4+}, Al^{3+} and Ca^{2+}, leached from low-calcium fly ash mixed with 5 different concentrations of NaOH solution (approximating the optimum dose range) and the corresponding variation trends over time. Moreover, we studied the changes in the mineral composition and surface morphology of the fly ash residues during alkali activation, and the results provide insights into the reaction processes and micro-mechanisms of alkali activation of low-calcium fly ash.

2 Experimental Procedures

2.1 Materials

The fly ash samples were collected from the Xingneng power plant (Shanxi Province, China). The specific gravity of the fly ash was 2.1 g cm^{-3}, and its specific surface area was 0.293 m^2 g^{-1}. Particle size analysis of the fly ash samples was conducted using a laser particle size analyzer (Mastersizer 2000, Malvern Instruments Ltd., Worcestershire, UK). The particle size distribution of the fly ash samples (Fig. 1) ranged from 0.286 to 457.1 μm, with the 0–1 μm fraction accounting for 1.17% of the sample, the 1–10 μm fraction accounting for 11.93%, the 10–100 μm fraction accounting for 59.88%, and the 100–460 μm fraction accounting for 27.02%.

The chemical components of the fly ash were determined using X-ray fluorescence spectrometry (XRF S8 TIGER, Bruker AXS Gmbh, Germany), and the fly ash was found to primarily consist of SiO_2 (58.14%), Al_2O_3 (30.03%), Fe_2O_3 (3.80%), CaO (3.58%) and MgO (2.53%). The major oxides SiO_2, Al_2O_3 and Fe_2O_3 presented a total content of over 70 wt%, and the CaO content of less than 10% indicated that these fly ash samples should be classified as Class F according to the definition in ASTM C 618. Figure 2 shows that the major mineralogical composition of the fly ash samples, determined via X-ray diffraction (XRD, Rigaku D/Max2500, Japan) analysis, consisted of quartz, mullite, and a noncrystalline vitreous phase.

The chemical reagent NaOH (Tianjin Chemical Works, > 96 wt%) was used as the alkaline activator. Deionized water was employed in the experiment.

2.2 Sample Preparation and Test Plan

(1) The fly ash samples collected at the power plant were placed in a 110 °C electric oven and dried for 12 h to a constant weight. These samples then were divided into 30 subsamples of 100 g each, which were weighed on an electronic balance with a precision of 0.0001 g.

(2) We prepared five 2400-mL NaOH solutions with concentrations of 0, 0.25, 0.75, 1.25 and 2 mol L^{-1},

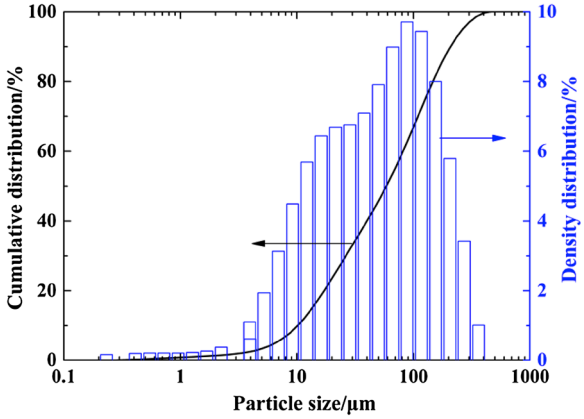

Fig. 1 Particle size distribution of the raw fly ash.

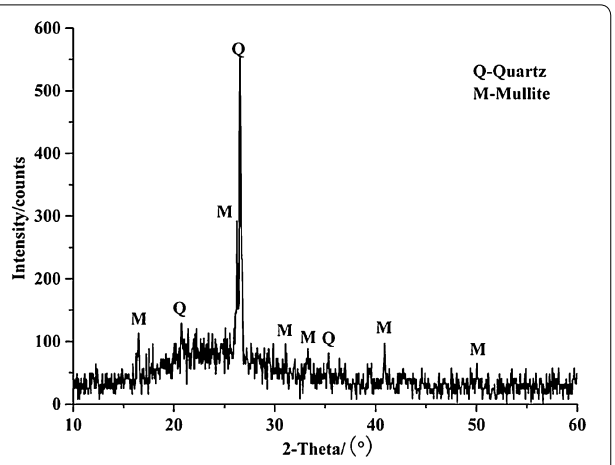

Fig. 2 X-ray diffraction pattern (XRD) of the raw fly ash.

(corresponding to NaOH doses in the filling material of 0, 1, 3, 5, and 8%, respectively, calculated based on the mass of water in the mixture), which were labeled A, B, C, D, and E, respectively. Then, each solution was divided into 6 portions of 400 mL, for a total of 30 aliquots that were stored separately in 1 L polyethylene bottles marked A1,…, E6.

(3) The fly ash samples from step (1) were successively transferred to polyethylene bottles, which were shaken for 5 min, sealed, and placed in a 25 °C water bath to maintain a constant temperature. The soaking times were 3, 6, 12, 24, 48 and 72 h, thereby generating the desired 30-sample test scheme (Table 1).

(4) The supernatants of the sample solutions were filtered through membrane filters (0.8 μm) to remove the undissolved fly ash. A total of 1 mL of each leaching solution was collected using pipettes with a 0.01 mL precision and diluted 1000-fold using deionized water in a stepwise manner to meet the test sample concentration requirements (< 40 ppm) of the ICP-OES instrument. The diluted solution was allowed to rest for 2 days in sealed polyethylene bottles, and no precipitates were found in any of the diluted solutions before analysis. Each sample was then prepared for the analysis of the Si^{4+}, Al^{3+} and Ca^{2+} ion concentrations.

(5) The fly ash residues (including unreacted or undissolved particles, particles under alkaline attack and reaction products) were collected after different soaking times and then washed three times with deionized water to remove the surface NaOH solution. Then, these residues were dried for 48 h in a 50 °C electric oven to a constant weight in preparation for analysis of the mineralogy, chemical functional groups and surface morphology.

2.3 Ion Leaching Test

ICP-OES (Thermo iCAP 6300, USA) was employed to determine the concentrations of Si^{4+}, Al^{3+} and Ca^{2+} in the leaching solutions described above after dilution and the measurement results of the sample have been investigated by the calibration curve method. The test included the following steps.

(1) A total of 6 mL was collected from each of the 30 leaching solutions after dilution and was divided into 3 aliquots of 2 mL each. Each of the 3 aliquots was placed in a separate 100 mL polyethylene volumetric flask.

(2) Then, 0.1 mL of 36% HNO_3 was added to two of the volumetric flasks from Step 1. Into one of these two flasks, 5 mL of an aluminum standard solution (0.1 mg mL^{-1}), 2 mL of a calcium standard solution (1 mg mL^{-1}) and 2 mL of a silicon standard solution (1 mg mL^{-1}) were successively added. This solution was subsequently diluted with secondary deionized water to a constant volume. Into the second flask, 10 mL of the aluminum standard solution (0.1 mg mL^{-1}), 4 mL of the calcium standard solution (1 mg mL^{-1}) and 4 mL of the silicon standard solution (1 mg mL^{-1}) were successively added,

Table 1 Ion leaching test scheme for alkali-activated low-calcium fly ash with different NaOH concentrations and soaking times.

NaOH concentration (mol L^{-1})	Solution volume (mL)	Fly ash samples (g)	Soaking time (h)					
			3	6	12	24	48	72
0	400	100	A_1	A_2	A_3	A_4	A_5	A_6
0.25	400	100	B_1	B_2	B_3	B_4	B_5	B_6
0.75	400	100	C_1	C_2	C_3	C_4	C_5	C_6
1.25	400	100	D_1	D_2	D_3	D_4	D_5	D_6
2	400	100	E_1	E_2	E_3	E_4	E_5	E_6

and this solution was then diluted with secondary deionized water to a constant volume to prepare the standard solution.

(3) In the remaining polyethylene volumetric flasks from Step 1, 0.1 mL of 36% HNO_3 was added, and the solution was then diluted to a constant volume with deionized water to prepare the sample solution.

(4) The instrument automatically adjusts to the initialized state. The three elements to be tested (Si, Al and Ca) and the corresponding spectral lines (251.612 nm for Si, 309.271 nm for Al and 393.366 nm for Ca) were selected from iTEVA software to begin the test. The standard solutions were tested first, and the three standard curves for Si, Al and Ca were drawn with the concentration as the abscissa and the intensity of the emission spectrum as the ordinate. Then, the sample solutions were run to determine the intensity of the emission spectra of the three elements on their own spectral lines and the corresponding absolute values of the abscissa on the standard curves, which were the concentrations of Si^{4+}, Al^{3+} and Ca^{2+} in the solutions. Each sample was tested in parallel three times under repeatable conditions and the coefficients of variation (CV) for the ion concentration measurements were less than 5%. The average value was taken as the result for comparison with the precision requirements.

(5) The leached amounts of Si^{4+}, Al^{3+} and Ca^{2+} were calculated according to Eq. (1):

$$W = \frac{C \times V \times d}{M} \tag{1}$$

where W is the amount of leached Si^{4+}, Al^{3+} or Ca^{2+} (mg g^{-1}); C is the average Si^{4+}, Al^{3+}, or Ca^{2+} concentration of the sample solution (mg L^{-1}); V is the volume of the leaching liquid (L); d is the dilution ratio; and M is the dose of fly ash (g).

The increase in the rate of leaching of the active ions under the alkali activation effect at different soaking times was calculated relative to that without alkali activation, according to Eq. (2):

$$G = \frac{W_{NaOH} - W_{water}}{W_{water}} \times 100\% \tag{2}$$

where G is the percentage of the increase in the leaching of Si^{4+}, Al^{3+} or Ca^{2+} (%); W_{NaOH} represents the amount of leached Si^{4+}, Al^{3+} and Ca^{2+} in the presence of NaOH solutions of different concentrations (Groups B, C, D and E; mg g^{-1}); and W_{water} represents the amount of leached Si^{4+}, Al^{3+} and Ca^{2+} in deionized water (Group A; mg g^{-1}).

2.4 Test of the pH Value of the Leaching Solution

A pH meter (PHS-3C Rex, China) was used to determine the pH value of the leaching solution at 25 °C. Prior to these measurements, the electrode was calibrated with a standard solution of borax (pH 9.18) and a mixed standard solution of potassium dihydrogenphosphate and disodium hydrogen phosphate (pH 6.86). The reported results are the average of three tests.

2.5 XRD Measurement

An XRD instrument (Rigaku D/Max2500, Japan) was used to determine the mineralogy of the fly ash residues. Under the test conditions, Cu was employed as the target, and Kα was used as the radiation, and the test specimens were step-scanned at 2θ values from 10 to 60°, with 0.05° steps and a rate of 0.5 s per step.

2.6 FTIR Measurement

A Fourier transform infrared spectroscopy instrument (FTIR, Thermo Fisher Nicolet iS5, USA) was used to characterize the chemical functional groups of the fly ash residues. FTIR is a key technique for the analysis of alkali-activated materials, particularly for low-calcium systems, in which it can probe the connectivity within Si–O–(Si, Al) frameworks via shifts in the peak corresponding to the asymmetric stretch of that bond (Provis et al. 2015). Before FTIR measurement, the pellet was dried for 12 h in a vacuum oven to minimize the effect of water on the spectrum. The FTIR spectra were determined by the potassium bromide (KBr) pellet method (1:100 wt% for the finely ground samples and KBr). The spectra were collected in the 400−4000 cm^{-1} wavenumber region with 32 scans at a resolution of 4 cm^{-1}.

2.7 SEM Measurement

Scanning electron microscopy (SEM, JEOL JSM-6700F, Japan), coupled with energy dispersive spectrometry (EDS, Oxford Instruments IET-200, UK), was employed to determine the surface morphology of the fly ash residues. The samples were sputter coated with a gold–palladium mixture before the assessment to reduce the interference of the negative charge during imaging.

3 Results and Analysis

3.1 Ion Leaching Behavior

3.1.1 Leaching Behavior of Si^{4+}

Figure 3a presents the trend of the amount of Si^{4+} leached over time from fly ash in NaOH solutions of different concentrations. According to the figure, in deionized

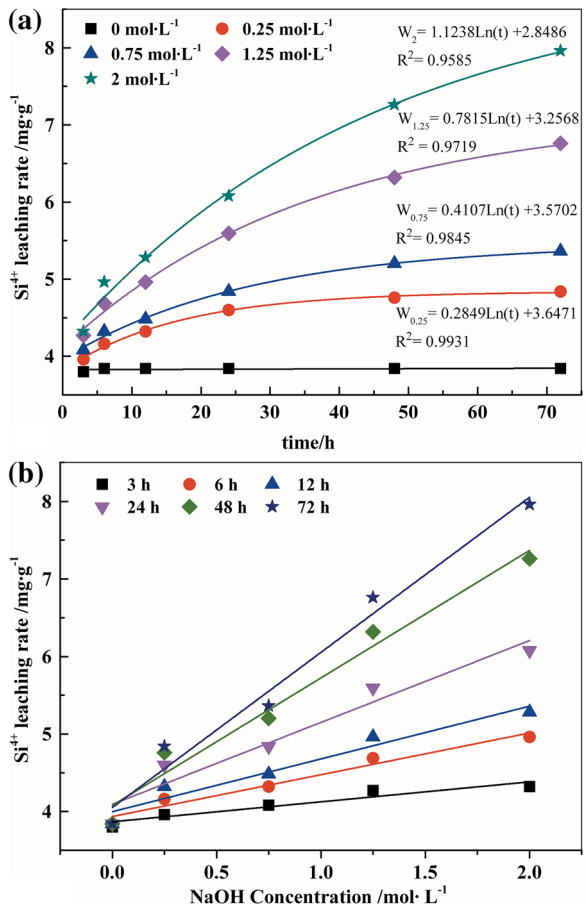

Fig. 3 Curves of the amount of leached Si^{4+} showing variations with **a** time and **b** NaOH concentration.

water, the amount of Si^{4+} leached reached 3.8 mg g^{-1} at 3 h then remained at 3.84 mg g^{-1} between 6 and 72 h. In the NaOH solution with a concentration of 0.25 mol L^{-1}, the amount of leached Si^{4+} increased from 3.96 mg g^{-1} at 3 h to 4.16, 4.32, 4.60, 4.76 and 4.84 mg g^{-1} at 6, 12, 24, 48 and 72 h, respectively. In the NaOH solutions with concentrations of 0.75, 1.25 and 2 mol L^{-1}, the amount of leached Si^{4+} increased from 4.08, 4.27 and 4.32 mg g^{-1} at 3 h to 5.36, 6.76 and 7.96 mg g^{-1} at 72 h, respectively. The results of fitting the test data showed that in the NaOH solutions with different concentrations, the amount of Si^{4+} leached increased according to a logarithmic curve over an extended time intervals. For a given time interval, the amount of Si^{4+} leached increased linearly with increases in the concentration of the NaOH solution, as shown in Fig. 3b.

3.1.2 Leaching Behavior of Al^{3+}

Figure 4a shows the trend of the amount of Al^{3+} leached over time from fly ash in NaOH solutions of different concentrations. The figure shows that in deionized water, the amount of leached Al^{3+} increased from 0.48 mg g^{-1} at 3 h to 0.85 mg g^{-1} at 6 h and then remained at 0.92 mg g^{-1} between 12 and 72 h. In the NaOH solution with a concentration of 0.25 mol L^{-1}, the amount of leached Al^{3+} increased from 0.61 mg g^{-1} at 3 h to 1.26, 1.48, 1.71, 1.95 and 2.03 mg g^{-1} at 6, 12, 24, 48 and 72 h, respectively. In the NaOH solutions with concentrations of 0.75, 1.25 and 2 mol L^{-1}, the amount of leached Al^{3+} increased from 1.55, 2.02 and 2.27 mg g^{-1} at 3 h to 2.49, 3.30 and 4.00 mg g^{-1} at 72 h, respectively. The results of fitting the test data showed that in NaOH solutions with different concentrations, the amount of leached Al^{3+} increased according to a logarithmic curve over extended time intervals. For a given time interval, the amount of leached Al^{3+} increased linearly with increases in the concentration of the NaOH solution, as shown in Fig. 4b.

3.1.3 Leaching Behavior of Ca^{2+}

Figure 5a shows the trend of the amount of Ca^{2+} leached over time from fly ash in NaOH solutions of different concentrations. According to the figure, in deionized water, the amount of leached Ca^{2+} increased slowly, from 0.62 mg g^{-1} at 3 h to 0.68 mg g^{-1} at 24 h, then remained at 0.68 mg g^{-1} between 24 and 72 h. In the NaOH solutions with concentrations of 0.25, 0.75, 1.25 and 2 mol L^{-1}, the amount of leached Ca^{2+} was 0.032 mg g^{-1} at 3 h and increased to 0.052, 0.048, 0.048 and 0.044 mg g^{-1} at 72 h, respectively. Figure 5b shows that the amount of leached Ca^{2+} in water was higher than in the NaOH solutions, because the leached Ca^{2+} reacted with OH^- to generate a $Ca(OH)_2$ precipitate (Provis et al. 2009). Because the concentration of OH^- in the water was much lower than in the NaOH solutions, only a limited amount of $Ca(OH)_2$ precipitate formed in the water. As a result, the amount of leached Ca^{2+} in the water was much greater than that in the NaOH solutions. Ca^{2+} was detected in the NaOH solutions because $Ca(OH)_2$ is slightly soluble in water and a small amount of calcium was released secondarily (Lee and Deventer 2002).

3.1.4 Analysis of the Differences in the Leaching Behaviors of Si^{4+}, Al^{3+} and Ca^{2+}

Although the alkali activation effect clearly increased the amounts of active ions leached from the low-calcium fly ash, the leaching trends for Si^{4+}, Al^{3+} and Ca^{2+} were different.

(1) The amounts of leached Si^{4+}, Al^{3+} and Ca^{2+} were ranked as follows: Si^{4+}>Al^{3+}>Ca^{2+}. Within 72 h, the maximum amount leached was 7.96 mg g^{-1} for Si^{4+}, 4 mg g^{-1} for Al^{3+} and 0.04 mg g^{-1} for Ca^{2+}, because the contents of silicon, aluminum

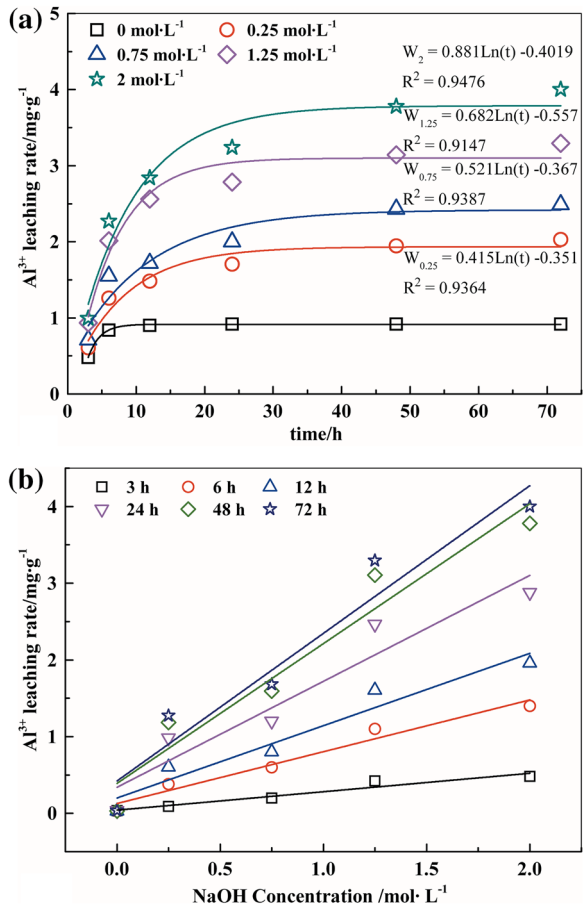

Fig. 4 Curves of the amount of leached Al^{3+} showing variations with **a** time and **b** NaOH concentration.

and calcium in the fly ash were different. The content of SiO_2 in the tested fly ash was 58.14%; the content of Al_2O_3 was 30.03%; and the content of CaO was only 3.58%.

(2) The amount of leached Ca^{2+} decreased with increases in the concentration of the NaOH solution, whereas the amounts of leached Si^{4+} and Al^{3+} increased with increases in the concentration of the NaOH solution. Therefore, the trend for Ca^{2+} was different from those for Si^{4+} and Al^{3+}, as Ca^{2+} generated a $Ca(OH)_2$ precipitate in the NaOH solution, which decreased the concentration of free Ca^{2+} with increasing concentration of the NaOH solution.

(3) Relative to that of the deionized water, the rates of increase in the leaching of Si^{4+}, Al^{3+} and Ca^{2+} from the fly ash varied among the NaOH alkali solutions. Table 2 shows the percent increases in the leaching of Si^{4+}, Al^{3+} and Ca^{2+} under the alkali activation effect after different soaking times relative to the condition without alkali activation. The results show that alkali activation increased the amount of leached Al^{3+} by 334.78% and that of leached Si^{4+} by 107.29%, whereas it produced a 92.53% decrease in the amount of leached Ca^{2+}. These results can be explained as follows: in the aluminosilicate structure of fly ash, Si–O mainly occurs in a tetra-coordinated tetrahedral structure with a stable nature, and Al–O occurs in a multi-coordinated polyhedral structure, which means that the Al–O–Si bonds are relatively weak compared with the Si–O–Si bonds (Xiao and Lasaga 1994). When the fly ash is attacked by the alkali solution, the bond energy of the Al–O bond is lower than that of Si–O, thus increasing the solubility of Al compared with Si. The decrease in the amount of leached Ca^{2+} was caused by the generation of a $Ca(OH)_2$ precipitate, thereby removing the Ca^{2+} from the NaOH solution.

3.2 Changes in the pH of the Leaching Solution

Figure 6 shows that the pH of the leaching solution changed over time. The pH value increased from 7.01 to 9.73 when fly ash was added to deionized water, followed by a slow downward trend, and the pH reached 9.35 at 72 h. The early rapid dissolution of the alkaline oxides in the fly ash led to an increase in the OH^- concentration in the system, thus increasing the pH value of the deionized water. The subsequent decrease in the pH value was related to the decrease in the amount of alkaline oxides dissolved in the later period and the consumption of OH^- in the formation of intermediate aluminosilicate material. In the NaOH solution with a concentration of 0.25 mol L^{-1}, the initial pH value was 12.9, and this pH changed to 12.75 after 72 h. At concentrations of 0.75, 1.25 and 2 mol L^{-1}, the initial pH values were 13.46, 13.69, and 13.97, respectively, and remained stable throughout the test period.

3.3 Changes in the Mineral Composition of the Fly Ash Residues

The XRD test results for the mineral composition of the fly ash residues soaked in the 2 mol L^{-1} NaOH solution are shown in Fig. 7. The XRD pattern of the raw fly ash shows high intensities corresponding to quartz and mullite. After alkali activation, some peaks in the XRD patterns changed with respect to the soaking time. The mineral components in the system did not change significantly after soaking for 12 h. The characteristic peak intensities of quartz and mullite of the samples that soaked for 72 h were lower than those of the raw fly ash, indicating that the alkali solution caused the destruction and dissolution of the crystalline structures of the quartz and mullite in the fly ash. After 168 h, the characteristic diffraction peaks of quartz and mullite were

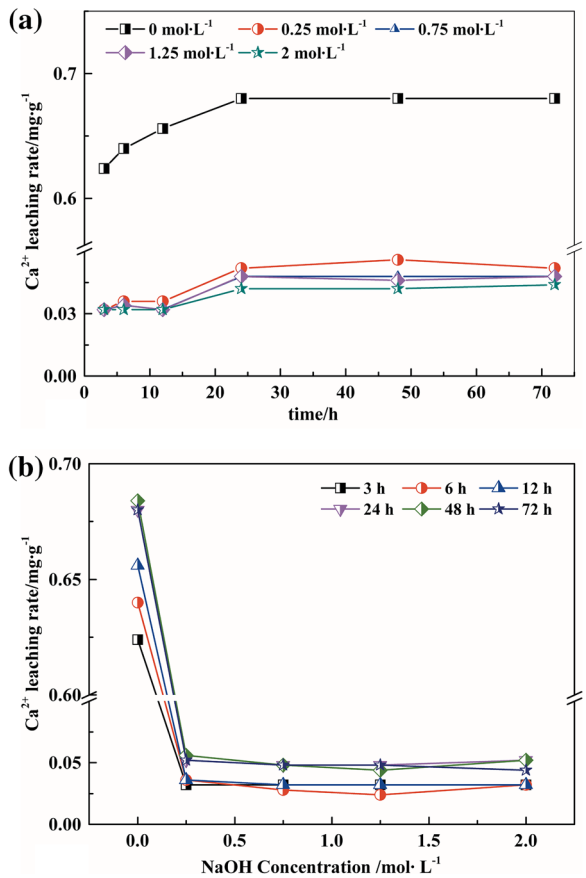

Fig. 5 Curves of the amount of leached Ca^{2+} showing variations with **a** time and **b** NaOH concentration.

significantly lower. The dispersed diffraction peaks of the noncrystalline-phase aluminosilicate glass in the raw fly ash became comparatively small after 672 h. Therefore, the destruction of the quartz and mullite crystalline structure continued under the action of alkali activation, and the noncrystalline-phase aluminosilicate glass was also attacked by the alkali solution. The XRD patterns of the samples show no significant formation of new peaks and no substantial crystallographic changes in the fly ash residues. In general, it is possible that the changes in the microstructure are related to amorphous sodium aluminosilicate hydrate (N–A–S–H) gel, which would be difficult to detect via XRD. Therefore, we performed FTIR and SEM analyses for further investigation.

3.4 Changes in the Functional Groups of the Fly Ash Residues

The FTIR spectra for the fly ash residues with different soaking times and different NaOH concentrations are shown in Fig. 8a, b, respectively. Both sets of FTIR spectra feature similar profiles and marked wavenumbers. A broad peak between 3432 and 3472 cm^{-1} is observed due to strong O–H stretching vibrations. Absorption bands at 1624–1634 cm^{-1} are assigned to the bending vibration of the O–H groups of the hydrated reaction products. Small bands were observed between 1400 and 1420 cm^{-1} and are associated with the stretching mode of O–C–O bonds in carbonate groups (Nadziri et al. 2017). The main binding gel of the NaOH-activated low-calcium fly ash is characterized by a peak in a characteristic region

Table 2 Percent increases in the leaching of Si^{4+}, Al^{3+} and Ca^{2+}.

Active ions	Time (h)	0.25 mol L^{-1}	0.75 mol L^{-1}	1.25 mol L^{-1}	2 mol L^{-1}
Si^{4+}	3	4.21	7.37	12.42	13.68
	6	8.33	12.50	22.08	29.17
	12	12.50	16.67	29.17	37.50
	24	19.79	26.04	45.63	58.33
	48	23.96	35.42	64.58	89.06
	72	26.04	39.58	76.04	107.29
Al^{3+}	3	26.67	48.33	95.00	106.67
	6	50.00	84.76	139.52	170.48
	12	64.89	91.11	184.44	215.56
	24	85.22	117.39	202.61	252.17
	48	111.30	164.35	241.74	310.87
	72	120.87	170.43	258.26	334.78
Ca^{2+}	3	− 94.9	− 94.9	− 94.9	− 94.9
	6	− 94.4	− 95.6	− 96.3	− 95.0
	12	− 94.5	− 95.1	− 95.1	− 95.1
	24	− 92.4	− 92.9	− 92.9	− 92.4
	48	− 91.8	− 93.0	− 93.6	− 92.4
	72	− 92.4	− 92.9	− 92.9	− 93.5

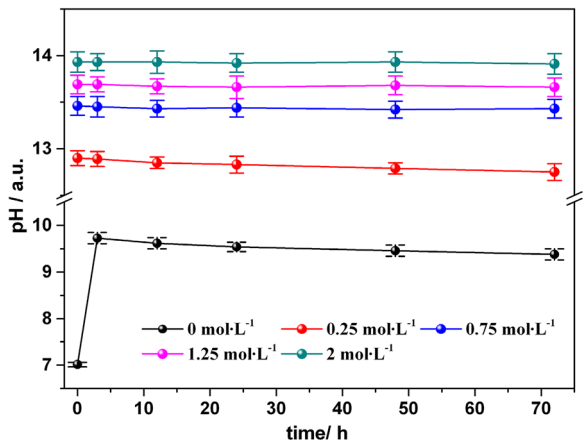

Fig. 6 Variation in pH values in the leaching solution with time (25 °C).

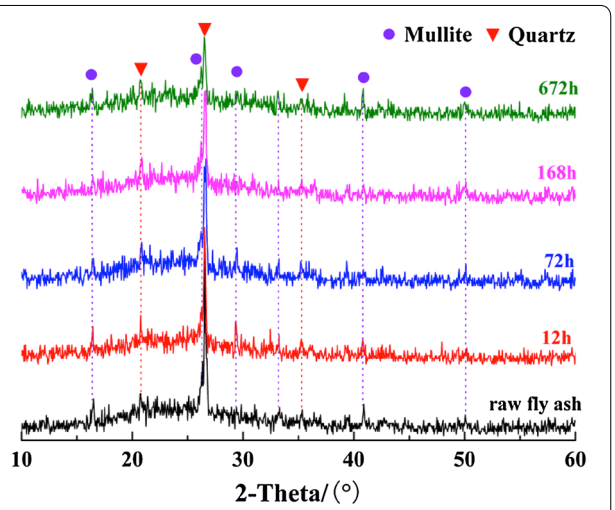

Fig. 7 XRD patterns of alkali-activated low-calcium fly ash treated with 2 M NaOH for 12, 72, 168 and 672 h.

(< 1300 cm^{-1}). The peak at a wavenumber of 1052 cm^{-1} in the raw fly ash shifts to a final position at approximately 1006 cm^{-1} in conjunction with a soaking duration of 336 h and approximately 1018 cm^{-1} in conjunction with NaOH solution concentration of 2 M, indicating a progressive reaction that is rich in silica gel. This shift is consistent with the formation of a sodium aluminosilicate-type gel (Zhang et al. 2012a; Vargas et al. 2014; Ismail et al. 2014; Nadziri et al. 2017). Alkali activation of low-calcium fly ash promotes the formation of more cross-linking in an aluminosilicate-type gel, which can be seen from the vibration in the band between 400 and 800 cm^{-1}. Slight shifts occur in the bending vibrations of Si–O–Si from 776 to 792 cm^{-1}, of Al–O–Al from 549 to 552 cm^{-1} and of Si–O–Si and O–Si–O from 460 to 425 cm^{-1} (Zhang et al. 2012b; Ismail et al. 2014). These results are consistent with the formation of an aluminosilicate gel containing Ca^{2+}, i.e., a C/N–A–S–H gel (I. Garcia-Lodeiro et al. 2011). As shown in Fig. 7a, b, significant differences exist among the FTIR spectrum changes near the 450 cm^{-1} wavelength with increasing soaking time and NaOH solution concentration. The FTIR results verify that the soaking times and alkali solution concentrations strongly influence the formation of hydration products during the alkali activation of low-calcium fly ash.

3.5 Changes in the Surface Morphology of the Fly Ash Residues

Figure 9 shows the test results from the SEM analysis of the changes in the morphological characteristics of the fly ash residues with different soaking times in a 2 mol L^{-1} NaOH solution. Figure 9 shows that a number of morphologies may coexist in the fly ash residues, including unreacted or undissolved ash particles, particles under alkaline attack, and precipitates (including reaction products). Among these morphologies, a significant number of unreacted or undissolved ash particles indicates a slower rate and lower proportion of reaction in the system.

The raw fly ash mainly consists of spherical particles of different sizes, and the surfaces of the particles are relatively smooth and exhibit good sphericity, with small amounts of tiny particles, such as debris and agglomerates, being attached to the surface (see Fig. 9a). Most of these tiny particles consist of materials such as soluble substances, quartz, mullite, and unburned coal (Brueggen et al. 2010). After soaking for 3 h, the surface of the particles gradually changed from smooth to rough, and some randomly scattered precipitates with a flaky structure (probably $Ca(OH)_2$) appeared on the surface of the particles (see Fig. 9b). After soaking for 72 h, the undissolved particle surface became rougher, and precipitates were continuously formed and precipitated in a disorderly manner on the particle surface (see Fig. 9c). The results of the EDS analysis showed that the main components of the precipitates were Si, Al, Na, and Ca (see Fig. 9d). Figure 9e shows that the hollow spheres of fly ash were filled with precipitates. After soaking for 672 h, Fig. 9f clearly shows that the surfaces of the undissolved fly ash particles were covered with a dense layer of precipitates, such as $Ca(OH)_2$ and zeolite. This image provides a reminder that the precipitation of the reaction products occurs continuously and that a layer of precipitates covering the undissolved particles would inhibit the activation of these particles. Additionally, some cracks in the layer can be observed in Fig. 9f, which might be

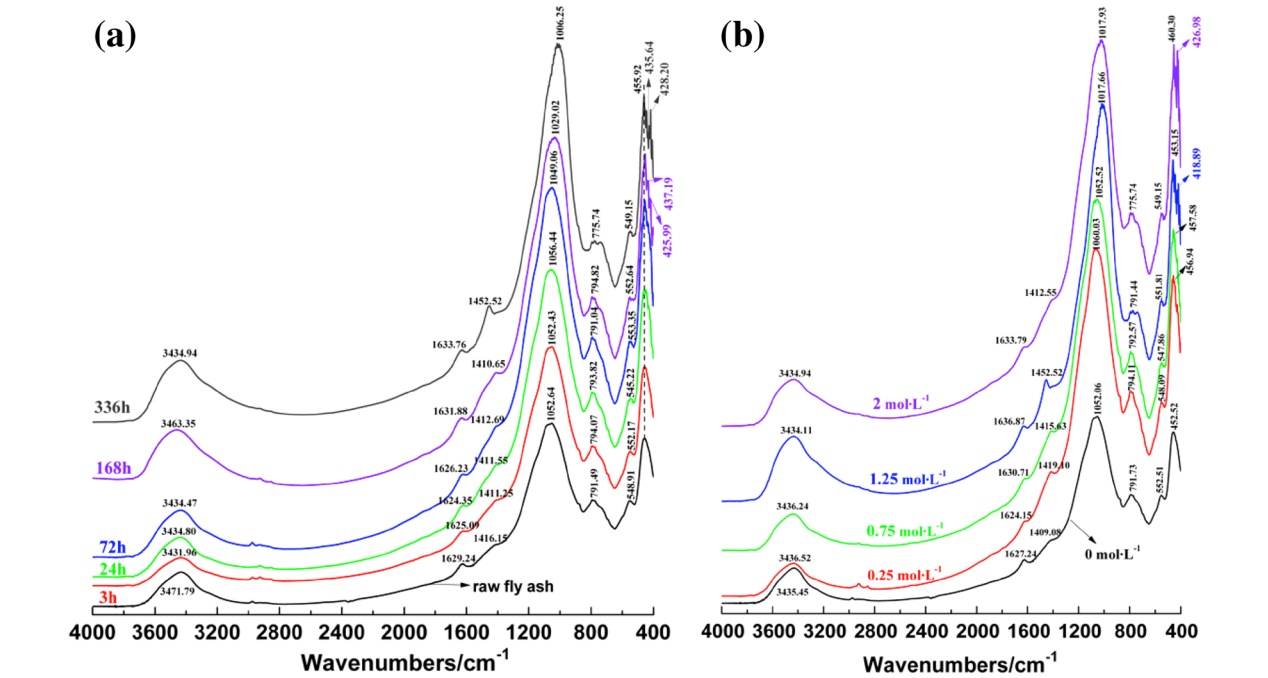

Fig. 8 FTIR spectra of alkali-activated low-calcium fly ash for different **a** soaking durations and **b** NaOH concentrations.

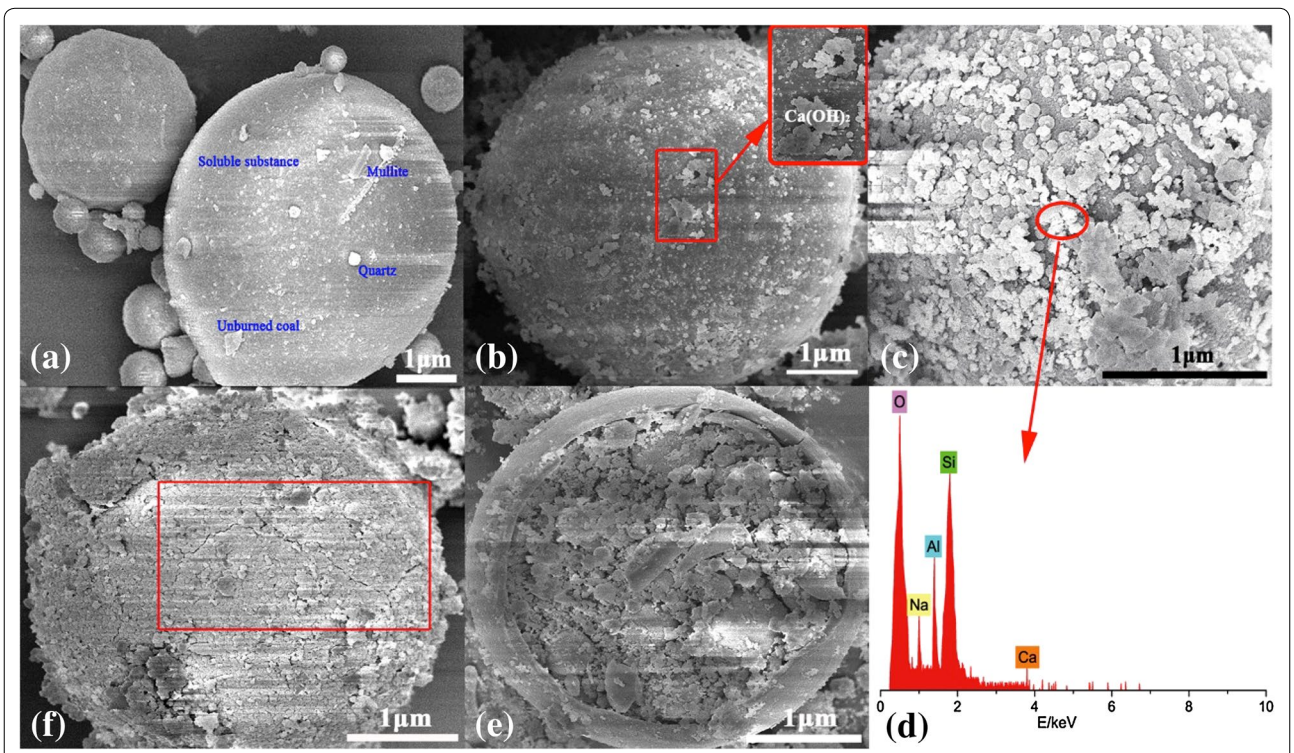

Fig. 9 SEM micrographs of alkali-activated low-calcium fly ash treated with 2 M NaOH for different soaking times: **a** raw fly ash, **b** 3 h, **c** 72 h, **d** EDS spectrum of precipitates, **e** hollow sphere, and **f** 672 h.

due to mechanical damage during sample preparation for SEM observation or could be caused by increases in the osmotic pressure of the interactions at phase boundaries, or could also be caused by internal moisture loss of hardened layer induced to drying shrinkage (Yan and Sagoe-Crentsil 2016).

4 Reaction Mechanism During Alkali Activation of Low-Calcium Fly Ash

Based on the above test and analytical results, the reaction mechanism during the alkali activation of low-calcium fly ash can be further interpreted. It was divided into four stages, as shown in Fig. 10, and is described below.

4.1 Dissolution Stage

The tiny soluble particles on the surface of the fly ash particles dissolved upon contact with the alkali/water solution and released a series of active ions, such as Si^{4+}, Al^{3+}, Ca^{2+}, and Mg^{2+} (Fig. 10a). The chemical reaction equations (Eqs. (3)–(8)) for the dissolution of the soluble solid particles at 25 °C are shown in Table 3, and the molar Gibbs free energy of the chemical reactions can be calculated using the standard molar Gibbs function. The calculation results showed that the molar Gibbs free energies of all of the above reactions were less than zero, indicating that the chemical reactions proceeded spontaneously. Moreover, the amount of tiny fly ash particles less than 1 μm in size (which accounted for approximately 1.17% of the total) that dissolved increased with increases in both the soaking time and NaOH concentration. Despite the relatively low percentage of these particles, the amounts were sufficient to significantly increase the ion concentrations in the solutions (Garcialodeiro et al. 2016). Consequently, an increased amount of tiny fly ash particles in the system increases the likelihood of achieving a better alkali activation effect, especially in the early period.

4.2 Depolymerization Stage

Figure 10b shows the depolymerization process of the fly ash particles under alkaline attack (note that in this figure, the aluminosilicate vitreous chain structure resulting from alkali attack may have been slightly exaggerated for effect). The addition of the alkali metal hydroxides results in a change in the ionic strength of the solution, which causes a redistribution of the electronic density around the chain structure (Glukhovsky 1965). The OH^- anions react with the surface of the fly ash particles via chemical hydration reactions, which causes the aluminosilicate network structure to break down and different complexes to form, such as $Al(OH)_4^-$ or $Al(OH)_6^{3-}$ and $SiO(OH)_3^-$, $SiO(OH)_2^{2-}$ or $SiO_3(OH)^{3-}$. The actual complex that forms depends on the alkali concentration in the solution (Swaddle et al. 1994; Xu and Deventer 2000). Furthermore, the alkali metal cation Na^+ is dispersed throughout the aluminosilicate network structure. When the aluminosilicate network structure is depolymerized, Na^+ neutralizes the excess charge via a physical electrostatic reaction, thereby generating Si–O–Na^+ bonds and hindering the reversibility of the reaction (Shi et al. 2011).

4.3 Polycondensation and Polymer Gel Stage

After depolymerization occurs and unstable ionic monomers form, the active Al^{3+} and Si^{4+} ions react under catalysis by OH^- to form nuclei in silicate and aluminate species consisting of SiO_4 and AlO_4 tetrahedra. Polycondensation between the silicate and aluminate species occurs more readily because of the characteristic high activity of $[Al(OH)_4]$, as shown in the following reaction:

$$[SiO_2(OH)_2]^{2-} + [Al(OH)_4]^- \rightarrow [(OH)_3Al - O - SiO_2(OH)]^{3-} + H_2O \quad (9)$$

$$[SiO(OH)_3]^- + [Al(OH)_4]^- \rightarrow [(OH)_3Al - O - SiO(OH)_2]^{2-} + H_2O \quad (10)$$

The reaction described by Eq. (9) tends to form dimers and trimers, whereas that described by Eq. (10) tends to form larger oligomers and polymers. The above reactions show that aluminate and silicate species are linked to each other by the attraction between the hydroxyl groups of the aluminate and silicate monomers, thereby forming an intermediate complex. The two hydroxyl groups in the intermediate complex subsequently condense to form an aluminosilicate species by releasing an H_2O molecule. This type of polycondensation reaction is usually a nucleophilic substitution reaction (Weng and Sagoe-Crentsil 2007). Thereafter, the aluminosilicate oligomers and the alkali metal cation Na^+ are further polycondensed via the action of a coordination bond or an electrostatic bond to form aluminosilicate gel, which accumulates gradually. As shown in Fig. 10c, the precipitates (e.g., $Ca(OH)_2$, aluminosilicate gel, etc.) precipitated on the surface of the fly ash particles are disordered after their formation.

4.4 Diffusion Stage

The precipitates eventually cover the surface of the undissolved particles, thereby hindering contact between the fly ash and the alkaline solution. This situation is unfavorable for the continued alkaline activation of the fly ash and gradually reduces the rate of alkali activation. Once the particles are completely covered by the precipitates, alkali attack occurs only via diffusion. Figure 10d illustrates the mechanism of the bidirectional diffusion of

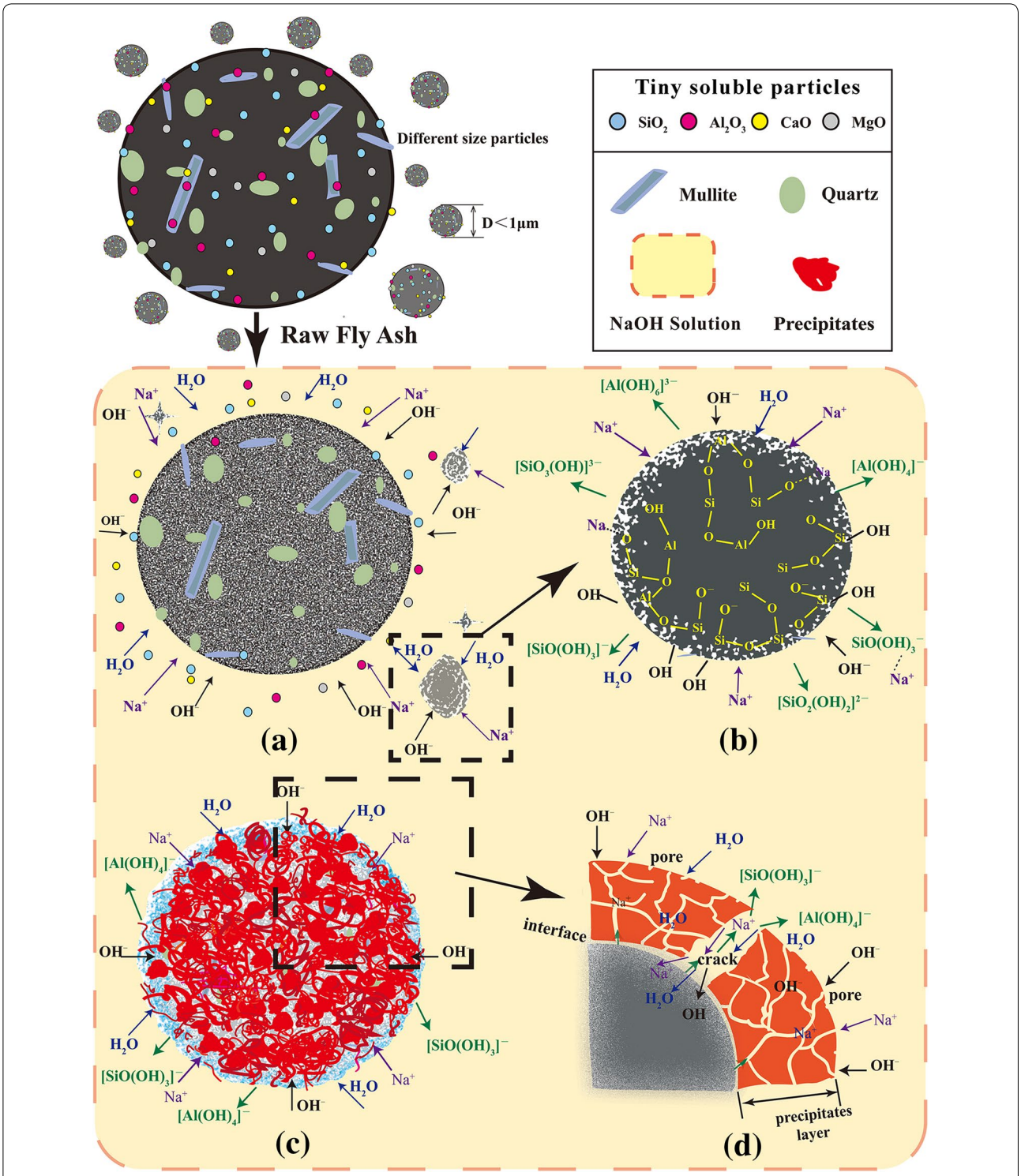

Fig. 10 Schematic diagram of the reaction mechanism during alkali activation of low-calcium fly ash: **a** dissolution stage, **b** depolymerization stage, **c** polycondensation and polymer gel stage, and **d** diffusion stage.

Table 3 Reaction equations for the soluble particles and their molar Gibbs free energy values (Zhang 2008; Liang 2007).

Oxides	Chemical reaction equations		$\Delta_r G_m^{\Theta}$ (298.16K) (kJ mol^{-1})
Alkaline oxides	$CaO(s) + H_2O \rightarrow Ca^{2+}(aq) + 2OH^-(aq)$	(3)	− 26.76
	$Ca^{2+}(aq) + 2OH^-(aq) \rightarrow Ca(OH)_2(s)$	(4)	− 30.00
	$MgO(s) + H_2O \rightarrow Mg^{2+}(aq) + 2OH^-(aq)$	(5)	− 37.79
	$Mg^{2+}(aq) + 2OH^-(aq) \rightarrow Mg(OH)_2(s)$	(6)	− 76.45
Acid oxides	$SiO_2(s) + H_2O + OH^-(aq) \rightarrow SiO(OH)_3^-(aq)$	(7)	− 26.25
	$Al_2O_3(s) + 3H_2O + 2OH^-(aq) \rightarrow 2Al(OH)_4^-(aq)$	(8)	− 41.86

alkali-activated fly ash. Figure 10d clearly shows that Na^+ and OH^- continue to attack the fly ash along the cracks and pores in the precipitate layer, while ionic silicon and aluminum monomers flow outward along these cracks and pores.

The mechanism of alkali activation of low-calcium fly ash is a consequence of a chemical reaction, which the reaction yields an inorganic polymeric-like material; bonded covalently and possessing favorable chemical and physical properties (Khalifeh et al. 2016). The results show that the progress of the reaction is controlled by dissolution in the early stages, whereas activation is governed by diffusion when the surfaces of the fly ash particles are covered by precipitates.

5 Conclusions

The NaOH concentration and soaking time have clear effects on the amount of active ions leached from low-calcium fly ash. At different NaOH concentrations, the amounts of leached Si^{4+} and Al^{3+} ions increased according to a logarithmic curve over an extended time period, whereas for a given time interval, the amounts leached increased linearly with increasing concentration of the NaOH solution. Alkali activation increased the amounts of leached Al^{3+} and Si^{4+} by 334.78 and 107.29%, respectively, relative to the condition without alkali activation. Ca^{2+} generates a $Ca(OH)_2$ precipitate in the NaOH solution, which explains why the amount of leached Ca^{2+} is high in water and low in the NaOH solution.

OH^- forms different complexes via chemical hydration reactions with fly ash, and aluminosilicate gel is formed after the polycondensation reaction with alkali metal cations, such as Na^+, via the action of a coordination bond or an electrostatic bond when low-calcium fly ash is soaked in an NaOH solution.

The alkali activator mainly affected the surface of the low-calcium fly ash particles and induced surface modifications that caused changes in the dissolution stage, depolymerization stage, polycondensation and polymer gel stage and diffusion stage. The effect of activation was related to the concentration of the alkaline solution, with higher concentrations leading to more significant effects. In addition, the characteristics of the fly ash, such as its fineness, vitreous content, mineral composition and chemical composition, also alter the effect of alkali activation.

Authors' contributions

BY conceived and designed the study, participated in discussing the results, drafted and revised the manuscript. TK contributed significantly to analysis and manuscript preparation. JK conducted the sample preparation and test work. YC acquired data and performed the data analyses. All authors read and approved the final manuscript.

Author details

[1] Institute of Mining Technology, Taiyuan University of Technology, Taiyuan 030024, China. [2] School of Mining and Technology, Inner Mongolia University of Technology, Hohhot 010051, China.

Acknowledgements

This work was funded by the National Natural Science Foundation of China (Grant Nos. 51174141 and 50974093). The authors would like to express their sincere thanks to the editors and anonymous reviewers for their valuable comments and insightful feedback.

Publisher's Note

Received: 19 October 2017 Accepted: 6 May 2018
Published online: 26 July 2018

References

Bijen, J., & Waltje, H. (1989). Alkali-activated slag–fly ash cements. In*Fly ash, silica fume, slag and natural Pozzolans in concrete. Proceedings of the third international conference.*

Blissett, R. S., & Rowson, N. A. (2012). A review of the multi-component utilisation of coal fly ash. *Fuel, 97,* 1–23.

Brueggen, B., Kang, T. H. K., & Ramseyer, C. (2010). Experimental and SEM analyses of ground fly ash in concrete. *International Journal of Concrete Structures & Materials, 4,* 51–54.

Çiçek, T., & Cincin, Y. (2015). Use of fly ash in production of light-weight building bricks. *Construction and Building Materials, 94,* 521–527.

Fernandez-Jimenez, A., García-Lodeiro, I., & Palomo, A. (2007). Durability of alkali-activated fly ash cementitious materials. *Journal of Materials Science, 42,* 3055–3065.

Fernández-Jiménez, A., & Palomo, A. (2005). Composition and microstructure of alkali activated fly ash binder: Effect of the activator. *Cement and Concrete Research, 35,* 1984–1992.

Garcialodeiro, I., Donatello, S., Fernándezjiménez, A., & Palomo, A. (2016). Hydration of hybrid alkaline cement containing a very large proportion of fly ash: A descriptive model. *Materials, 9,* 605.
Garcia-Lodeiro, I., Fernández-Jiménez, A., Palomo, A., & Macphee, D. E. (2011). Compatibility studies between N-A-S-H and C-A-S-H gels. Study in the ternary diagram Na_2O–CaO–Al_2O_3–SiO_2 –H_2O. *Cement and Concrete Research, 41*(9), 923–931.
Glukhovsky, V. D. (1965). Soil silicates, Their properties, technology and manufacturing and fields of application. Civil Engineering Institute, Kiev: PhD Dissertation.
Guerrero, A., Hernández, M., & Goñi, S. (2000). The role of the fly ash pozzolanic activity in simulated sulphate radioactive liquid waste. *Waste Management, 20,* 51–58.
Guo, C., Zou, J., Jiang, Y., Huang, T., Cheng, Y., & Wei, C. (2014). Thermal activation of coal fly ash by sodium hydrogen sulfate for alumina extraction. *Journal of Materials Science, 49,* 4315–4322.
Ismail, I., Bernal, S. A., Provis, J. L., Nicolas, R. S., Hamdan, S., & Deventer, J. S. J. V. (2014). Modification of phase evolution in alkali-activated blast furnace slag by the incorporation of fly ash. *Cement & Concrete Composites, 45*(1), 125–135.
Khalifeh, M., Saasen, A., Vrålstad, T., Larsen, H. B., & Hodne, H. (2015). Experimental study on the synthesis and characterization of aplite rock-based geopolymers. *Journal of Sustainable Cement-Based Materials, 5*(4), 233–246.
Khalifeh, M., Todorovic, J., Vrålstad, T., Saasen, A., & Hodne, H. (2016). Long-term durability of rock-based geopolymers aged at downhole conditions for oil well cementing operations. *Journal of Sustainable Cement-Based Materials, 6*(4), 217–230.
Kim, J. E., Park, W. S., Jang, Y. I., Kim, S. W., Kim, S. W., Nam, Y. H., et al. (2016). Mechanical properties of energy efficient concretes made with binary, ternary, and quaternary cementitious blends of fly ash, blast furnace slag, and silica fume. *International Journal of Concrete Structures & Materials, 10,* 97–108.
Kotwal, A. R., Kim, Y. J., Hu, J., & Sriraman, V. (2015). Characterization and early age physical properties of ambient cured geopolymer mortar based on class C fly ash. *International Journal of Concrete Structures & Materials, 9,* 35–43.
Lee, W. K. W., & Deventer, J. S. J. V. (2002). Structural reorganisation of class F fly ash in alkaline silicate solutions. *Colloids and Surfaces A: Physicochemical and Engineering Aspects, 211,* 49–66.
Liang H. (2007). Study on activity effect of fly ash. Central South University, Changsha: Master Degree Dissertation.
Luan, X. F., Pan, Z. H., & Wang, D. D. (2010). Study on the chemical activation of fly ash in fly ash blended portland cement system. *Bulletin of the Chinese Ceramic Society., 4,* 003.
Ma, Y., Hu, J., & Ye, G. (2012). The effect of activating solution on the mechanical strength, reaction rate, mineralogy, and microstructure of alkali-activated fly ash. *Journal of Materials Science, 47,* 4568–4578.
Nadziri, N., Ismail, I., & Hamdan, S. (2017). Binding gel characterization of alkali-activated binders based on palm oil fuel ash (pofa) and fly ash. *Journal of Sustainable Cement-Based Materials, 7,* 1–14.
Nikolić, V., Komljenović, M., Marjanović, N., Baščarević, Z., & Petrović, R. (2014). Lead immobilization by geopolymers based on mechanically activated fly ash. *Ceramics International, 40,* 8479–8488.
Palomo, A., Grutzeck, M. W., & Blanco, M. T. (1999). Alkali-activated fly ashes: A cement for the future. *Cement and Concrete Research, 29,* 1323–1329.
Provis, J. L., Palomo, A., & Shi, C. (2015). Advances in understanding alkali-activated materials. *Cement and Concrete Research, 78,* 110–125.
Provis, J. L., Rose, V., Bernal, S. A., & Van Deventer, J. S. (2009). High-resolution nanoprobe X-ray fluorescence characterization of heterogeneous calcium and heavy metal distributions in alkali-activated fly ash. *Langmuir, 25,* 11897–11904.
Purdon, A. (1940). The action of alkalis on blast-furnace slag. *Journal of the Society of Chemical Industry, 59,* 191–202.
Qian, M. G., Miao, X. X., & Jia-Lin, X. U. (2007). Green mining of coal resources harmonizing with environment. *Meitan Xuebao/Journal of the China Coal Society, 32,* 1–7.
Rashad, A. M. (2014). A comprehensive overview about the effect of nano-SiO 2 on some properties of traditional cementitious materials and alkali-activated fly ash. *Construction and Building Materials, 52,* 437–464.
Roychand, R., Silva, S. D., Law, D., & Setunge, S. (2016). Micro and nano engineered high volume ultrafine fly Ash cement composite with and without additives. *International Journal of Concrete Structures & Materials, 10,* 113–124.
Shi, C. (1996). Early microstructure development of activated lime-fly ash pastes. *Cement and Concrete Research, 26,* 1351–1359.
Shi, C. (2001). An overview on the activation of reactivity of natural Pozzolan. *Canadian Journal of Civil Engineering, 28,* 778–786.
Shi, C., & Day, R. L. (1993). Chemical activation of blended cements made with lime and natural pozzolans. *Cement and Concrete Research, 23,* 1389–1396.
Shi, C., Jiménez, A. F., & Palomo, A. (2011). New cements for the 21st century: The pursuit of an alternative to Portland cement. *Cement and Concrete Research, 41,* 750–763.
Shi, C., Krivenko, P., & Roy, D. (2005). *Alkali-activated cements and concretes*. Abingdon, UK: Taylor & Francis Group.
Swaddle, T. W., Salerno, J., & Tregloan, P. A. (1994). Aqueous aluminates, silicates, and aluminosilicates. *Chemical Society Reviews, 23,* 319–325.
Tango, E. (1992). Some studies on the activation of blast furnace slag in cements without clinker. In *Proceedings of the 9th international congress on the chemistry of cement* (pp. 101–106).
Vargas, A. S. D., Molin, D. C. C. D., Masuero, Ângela B., Vilela, A. C. F., Castro-Gomes, J., & Gutierrez, R. M. D. (2014). Strength development of alkali-activated fly ash produced with combined naoh and ca(oh)2 activators. *Cement & Concrete Composites, 53*(10), 341–349.
Weng, L., & Sagoe-Crentsil, K. (2007). Dissolution processes, hydrolysis and condensation reactions during geopolymer synthesis: Part I—low Si/Al ratio systems. *Journal of Materials Science, 42,* 2997–3006.
Xiao, Y., & Lasaga, A. C. (1994). Ab initio quantum mechanical studies of the kinetics and mechanisms of quartz dissolution: OH—catalysis. *Geochimica et Cosmochimica Acta, 60,* 2283–2295.
Xie, Z., & Xi, Y. (2001). Hardening mechanisms of an alkaline-activated class F fly ash. *Cement and Concrete Research, 31,* 1245–1249.
Xu, H., & Deventer, J. S. J. V. (2000). The geopolymerisation of alumino-silicate minerals. *International Journal of Mineral Processing, 59,* 247–266.
Yan, S., & Sagoe-Crentsil, K. (2016). Evaluation of fly ash geopolymer mortar incorporating calcined wastepaper sludge. *Journal of Sustainable Cement-Based Materials, 5*(6), 370–380.
Zhang, Y. (2008). *Physical Chemistry*. Bei Jing: Chemical Industry Press.
Zhang, J. B., Li, S. P., Li, H. Q., & He, M. M. (2016). Acid activation for pre-desilicated high-alumina fly ash. *Fuel Processing Technology, 151,* 64–71.
Zhang, Z. H., Wang, H., & Provis, J. (2012a). Quantitative study of the reactivity of fly ash in geopolymerization by FTIR. *Journal of Sustainable Cement-Based Materials, 1*(4), 154–166.
Zhang, Z. H., Wang, H., & Provis, J. L. (2012b). The reactivity of fly ash in geopolymer synthesis: a qualification study by FTIR. *Japanese Journal of Applied Physics, 54*(8), 082601.
Zhuang, X. Y., Chen, L., Komarneni, S., Zhou, C. H., Tong, D. S., Yang, H. M., et al. (2016). Fly ash-based geopolymer: clean production, properties and applications. *Journal of Cleaner Production, 125,* 253–267.